ANALYSIS OF CAVITY SHEDDING AROUND THE TWISTED HYDROFOIL

by

Jianbo ZANG[a], Hu ZHANG[a,b*], Jiean SHEN[a], and Yaoyao WANG[a]

[a] School of Mechanical Technology, Wuxi Institute of Technology, Wuxi, China
[b] Research Center of Fluid Machinery Engineering and Technology, Jiangsu University, Zhenjiang, China

Original scientific paper
https://doi.org/10.2298/TSCI220606180Z

In order to understand the mechanism of cavity shedding and evolution, turbulent cavitating flows of the twisted hydrofoil were numerically investigated using the k-ε turbulence model and the ZGB cavitation model. The results of the numerical calculation and the experimental method are basically consistent, which confirms the feasibility of the numerical calculation model. This study has obtained the following conclusions. Firstly, the cavity shedding can be summarized into six stages, and the cavity shape, pressure and velocity field at different stages are displayed, analyzed and compared in detail. Secondly, the shedding of cavity and its evolution are mainly caused by the re-entrant jet and side-entrant jet, in which the former provides the kinetic energy and the latter plays the role of guiding the direction. Thirdly, under the convective shearing action of the re-entrant jet and the main flow, a strong vortex located in the mid-back edge of the hydrofoil is formed, which promotes the transformation of the cavity shape into a U-shaped structure.

Key words*: numerical simulation, twisted hydrofoil, cavity shedding, U-shaped cavity, re-entrant jet, side-entrant jet*

Introduction

Cavitation is a complex phenomenon involving phase transformation, multi-scale turbulence and unsteadiness. Its generation, development and dissapation process will lead to a series of problems such as hydro-mechanical noise, vibration and cavitation erosion, which will greatly affect the performance and life of equipment. Therefore, it is extremely important to study the generation and dissapation of the cavities. The cavity evolution of hydraulic machinery such as axial-flow pump and propeller is complicated, changeable and difficult to analyze. However, as the basic component of complex mechanical structure, the cavity evolution around the hydrofoil is relatively simple and easy to analyze. The research on hydrofoil is conducive to the subsequent research on the cavity evolution of complex mechanical structure.

Foeth [1, 2] designed a special twisted hydrofoil, belonging to the relatively common hydrofoil, which has a more obvious and typical process of the cavity shedding. Through experimental observation, it is believed that cavity shedding is mainly caused by the re-entrant jet, along with the auxiliary effect of the side-entrant jet, but the reasons for these jets forming are not explained. On this basis, Li [3] and Maquil [4] used *k-ω* model to simulate and proved the existence of re-entrant jet and side-entrant jet, but there is no further discovery. Bensow [5] conducted simulation using RANS, DES, and LES, respectively, and believed that LES and modified RANS have better effects. Luo *et al.* [6] and Ji *et al.* [7-9] conducted experimental research and

* Corresponding author, e-mail: zhanghutianxia@126.com

LES, PANS simulation of twisted hydrofoil, and confirmed the important role of confirming the re-entrant and side-entrant jets on the cavity. At the same time, the pressure pulsation caused by cavity shedding was emphasized, and the pulsation was the largest in the middle part of the hydrofoil, which happened to be the location of cavity accumulation, indicating that cavity shedding will produce large pulsation and damage to the hydrofoil. Pan [10] and Zhang [11] used the DCM FBM turbulence model to simulate, which required less computational force, and the simulation results were consistent with the experimental phenomenon, simultaneously, the re-entrant jet and side-entrant jet were also captured. Liu and Wang [12] used the non-linear k-ε turbulence model and found that it was in agreement with the experimental data. Wang *et al*. [13] used RNG model to analyze pressure fluctuation of cavity shedding. Authors in [14-16] mentioned that U-shaped vortexes are closely related to cavity shedding in the simulation. Asnaghi and Bensow [17] used Ω method to explain the relationship between cavity shedding and vortex, and U-shaped vortexes were emphasized. Hu *et al*. [18] analyzed the influence of the leading edge roughness on the flow field, which indirectly affected cavitation. Yin *et al*. [19] compared the cavitation phenomenon of two hydrofoils and emphasized the interaction between shedding dynamics and turbulent waves. Yu *et al*. [20] analyzed the characteristics of cavitation flow in combination with time and space.

The aforementioned investigations have described the shedding mechanisms of cavity around the twisted hydrofoil in a relatively comprehensive way, but the methods adopted have poor visibility in the display of the re-entrant jet and side-entrant jet, and the evolution of cavitation after shedding is hardly involved. On the basis of previous studies, this article adopts better approaches to express the effects that the re-entrant and side-entrant jet make on cavity in different stages, and studies the evolution process and mechanisms of the cavity, especially the U-shaped cavity formed after it shed. Simultanously, this article elaborates on the lifecycle of the cavity, and lays a solid foundation for the follow-up research on cavity shedding of auxiliary hydraulic machinery such as axial-flow pump.

The simulation method

The geometric model

This paper adopts the 3-D twisted hydrofoil Twist-11EPFL invented by Delft University of Technology [2]. The section of Twist-11EPFL is NACA0009 hydrofoil, chord length c = 0.15 m, wingspan y = 0.3 m. The hydrofoil is symmetrical about the middle section of the wingspan.

The spanwise variation of hydrofoil attack angle satisfies the equation [2]:

$$\alpha = 11\left(2\left|\frac{y}{150}-1\right|^3 - 3\left|\frac{y}{150}-1\right|^2 + 1\right) - 2 \tag{1}$$

The geometric model and span-wise distribution of attack angle of the hydrofoil are shown in fig. 1.

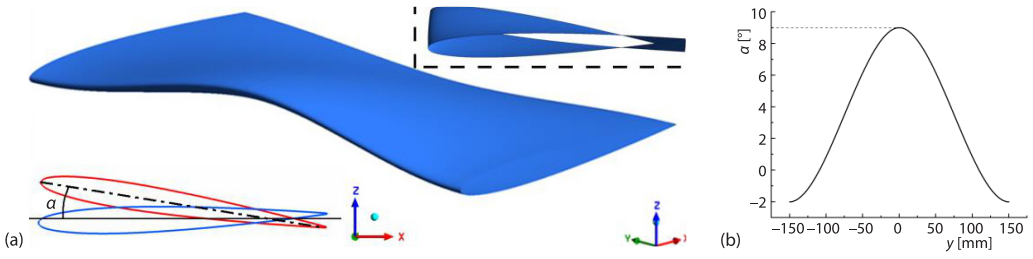

Figure 1. (a) The geometric model and (b) span-wise distribution of attack angle

Numerical calculation mode

The cavitating turbulent flows were modeled based on the homogeneous assumption, in which the multi-phase flows of the liquid and vapor were considered to share the same velocity and pressure. The continuity and momentum equations for the mixture flow are expressed:

$$\frac{\partial \rho}{\partial t}+\frac{\partial(\rho u_j)}{\partial x_j}=0 \tag{2}$$

$$\frac{\partial(\rho u_i)}{\partial t}+\frac{\partial(\rho u_i u_j)}{\partial x_j}=-\frac{1}{\rho}\frac{\partial p}{\partial x_i}+\frac{1}{\rho}\frac{\partial}{\partial x_j}\left[(\mu+\mu_t)\left(\frac{\partial u_i}{\partial x_j}+\frac{\partial u_j}{\partial x_i}-\frac{2}{3}\frac{\partial u_k}{\partial x_k}\delta_{ij}\right)\right] \tag{3}$$

where u_i is the velocity component in the i^{th} direction, p – the pressure, and μ_t – the turbulent viscosity. The dynamic viscosity μ and density ρ were defined:

$$\rho=\alpha_v\rho_v+(1-\alpha_v)\rho_\ell \quad \text{and} \quad \mu=\alpha_v\mu_v+(1-\alpha_v)\mu_\ell$$

respectively, where the subscripts ℓ and v represent the liquid and vapour phases, respectively, and α_v is the vapor volume fraction.

In order to get the value of μ_t which needed by momentum eq. (3), k-ε two-equation model is introduced. Turbulence dissipation rate ε is defined:

$$\varepsilon=\frac{\mu}{\rho}\left(\frac{\partial \overline{u}_i'}{\partial x_k}\right)\left(\frac{\partial \overline{u}'}{\partial x_k}\right)$$

the turbulent viscosity μ_t can be expressed as a function of k and ε:

$$\mu_t=\rho C_\mu\frac{k^2}{\varepsilon}$$

The k equation including turbulent kinetic energy in the k-ε model is defined:

$$\frac{\partial(\rho k)}{\partial t}+\frac{\partial}{\partial x_j}(\rho u_j k)=\frac{\partial}{\partial x_j}\left[\left(\mu+\frac{\mu_t}{\sigma_k}\right)\frac{\partial k}{\partial x_j}\right]+P_k-\rho\varepsilon+P_{kb} \tag{4}$$

The turbulent dissipation rate ε equation is given:

$$\frac{\partial(\rho\varepsilon)}{\partial t}+\frac{\partial}{\partial x_j}(\rho u_j\varepsilon)=\frac{\partial}{\partial x_j}\left[\left(\mu+\frac{\mu_t}{\sigma_\varepsilon}\right)\frac{\partial \varepsilon}{\partial x_j}\right]+\frac{\varepsilon}{k}\left(C_{\varepsilon 1}P_k-C_{\varepsilon 2}\rho\varepsilon+C_{\varepsilon 1}P_{\varepsilon b}\right) \tag{5}$$

where P_{kb} and $P_{\varepsilon b}$ are the influence of buoyancy in k and ε equations, respectively and P_k is the turbulence generation term caused by viscous force, expressed:

$$P_k=\mu_t\left(\frac{\partial u_i}{\partial x_j}+\frac{\partial u_j}{\partial x_i}\right)\frac{\partial u_i}{\partial x_j} \tag{6}$$

In the standard k-ε model, $C_\mu=0.09$, $C_{\varepsilon 1}=1.44$, $C_{\varepsilon 2}=1.92$, $\sigma_\varepsilon=1.3$, and $\sigma_k=1.0$.

The ZGB cavitation model, proposed by Zwart [21], considered that when the vapour volume fraction increases, the vapour nucleus density decreases correspondingly, and $\alpha_{nuc}(1-\alpha_v)$ is used to replace α_v. The mass transfer expression between evapouration $\dot{m}^+$ and condensation $\dot{m}^-$ phases is defined:

$$\frac{\partial(\rho_v\alpha_v)}{\partial t}+\frac{\partial(\rho_v\alpha_v u_j)}{\partial x_j}=\dot{m}^+-\dot{m}^- \tag{7}$$

$$\dot{m}^{+} = F_{\text{vap}} \frac{3\alpha_{\text{nuc}}\left(1-\alpha_{\text{v}}\right)\rho_{\text{v}}}{R_b}\sqrt{\frac{2}{3}\frac{p_{\text{v}}-p}{\rho_\ell}},\ \ p \le p_{\text{v}} \tag{8}$$

$$\dot{m}^{-} = F_{\text{cond}} \frac{3\alpha_{\text{nuc}}\rho_{\text{v}}}{R_b}\sqrt{\frac{2}{3}\frac{p_{\text{v}}-p}{\rho_\ell}},\ \ p > p_{\text{v}} \tag{9}$$

where $\alpha_{\text{nuc}}=5 \cdot 10^{-4}$, The radius of a single bubble $R_b = 2 \cdot 10^{-6}$ m, evapouration coefficient $F_{\text{vap}} = 300$, and condensation coefficient $F_{\text{cond}} = 0.03$.

The commercial code ANSYS CFX 17.1, which is widely used in engineering applications, was adopted in this study [22].

Compute domain and boundary conditions

The boundary conditions are velocity inlet and average static pressure outlet, the inlet velocity V_0 = 6.97 m/s, the outlet static pressure is 29 kPa, the saturated vapour pressure of water p_{v} = 3574 Pa, cavitation number $\sigma = (p - p_{\text{v}}) / (0.5\rho V_0) = 1.07$, the turbulence model is k-ε model, the telescopic wall function, the time step $\Delta t = 1.076 \cdot 10^{-4}$ s^{-1}, The number of inner cycles selected in each time step is 10. Symmetrical boundary conditions are adopted at the mid-section in the spanwise direction, and solid-wall no-slip conditions are adopted for walls of tunnel and hydrofoil surfaces, fig. 2. The convective term uses high resolution, the transient time term is second-order backward Euler, the turbulence term has first-order numerical accuracy, and the convergence accuracy is set to 10^{-4}.

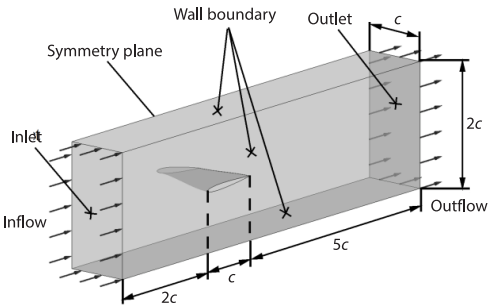

Figure 2. Compute domain and boundary conditions

Simulation accuracy verification

As shown in tab. 1, the average lift coefficient C_ℓ and average drag coefficient C_d are used as the standard of verification. Grid 2 shows the similar results with Grid 3. Considering numerical precision and resource consumption, Grid 2 is chosen for computation.

Table 1. The grid refinement test

Mesh	Nodes	C_ℓ	C_d
Grid 1	1257457	0.43828	0.02590
Grid 2	2514986	0.44017	0.02618
Grid 3	5026438	0.44031	0.02634

Experimental images of corresponding working conditions in Foeth's paper [2] are used to verify the accuracy of simulation. Experimental images of Twist-11EPFL provided by Foeth are divided into two groups, with the inlet velocity V_0 = 14 m/s and 6.75 m/s, respectively. In one period T, the images similar to the experiment phenomena are captured. The case of V_0 = 14 m/s is the top view as shown in fig. 3, and the case of V_0 = 6.75 m/s is the front view as shown in fig. 4:

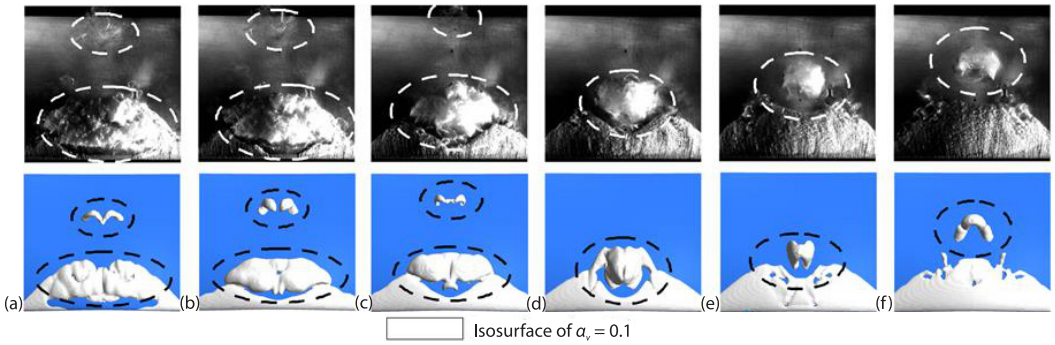

Figure 3. Top view of experimental simulation comparison (V_0 = 14 m/s)

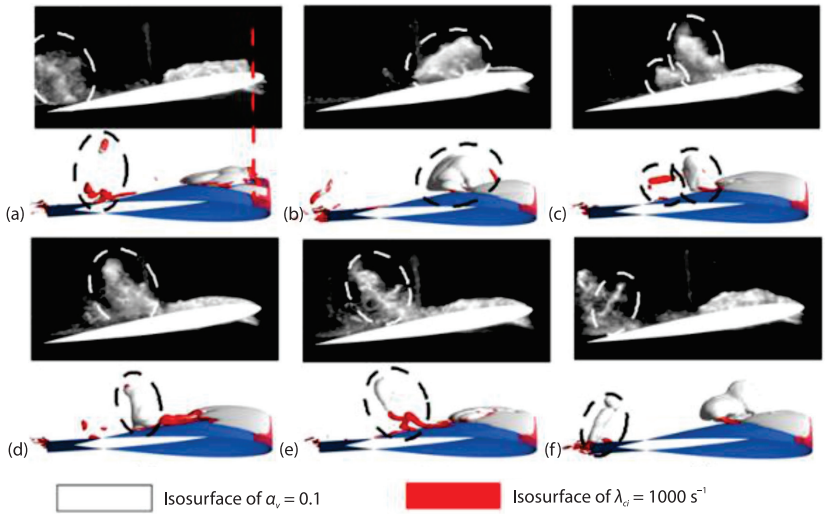

Figure 4. Front view of experimental simulation comparison (V_0 = 6.75 m/s)

Results and discussion

Process of cavity shedding

It is noted that english letters are used to classify the vapour bubbles in figs. 5 and 6, among which, the lowercase letters a, b, c, d represent the cavity that has not shed, and the capital letters A, B, C represent the cavity that has shed and separated from the main cavity.

The time from the inception of the main cavity shedding to its departure of the hydrofoil is defined as a period T, and the complete process from the formation of the Cavity B to its departure of the hydrofoil in fig. 5 is depicted. At $t + T/16$, the Cavity A just separates from the main cavity, and the remaining part of the main cavity is relatively complete, and there is no new formation of the shed Cavity B. At $t + 2T/16$, the main cavity side starts to crack and the Cavity b also begins to develop. In the subsequent evolution, the cracks gradually expand and deepen inside the main cavity, eventually to $t + 6T/16$, the cracks go through the main cavity, then the Cavity b breaks away from the main cavity, forming the independent shed Cavity B. Under the action of incoming flow, the Cavity B finally separates from the hydrofoil. It is worth noting that at $t + 9T/16$, shortly after the separation of the Cavity B, the main cavity begins to

collapse again, and the Cavity c begins to develop accordingly. Similarly, the Cavity d also starts to develop after the separation of the shed Cavity C.

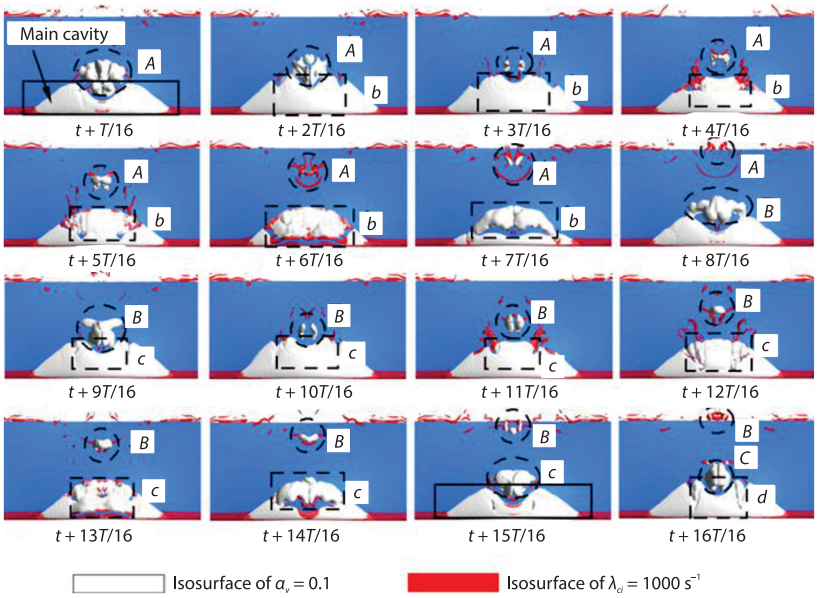

Figure 5. Simulation of cavitation evolution (top view)

The front view has a poor visibility of the process of the cavity shedding in fig. 6. However, for the evolution of the Cavity B after $t + 8T/16$, when it separates from the main cavity, the front view shows a clear shed cavity structure. It can be seen that in the process of $t + 6T/16 \sim t + 8T/16$, the Cavity B is originally tiled on the surface of the hydrofoil, then begins to move downstream. The circular structure B at $t + 8T/16$ gradually changes into a long strip structure at $t + 11T/16$. Meanwhile, at $t + 11T/16$, the top area of the shed Cavity B is behind the bottom area, but in the subsequent evolution of the movement, the velocities of both are great different. At $t + 15T/16$, the pattern of the Cavity B changes to the top being forward and the bottom being backward, which can also be captured in experiment.

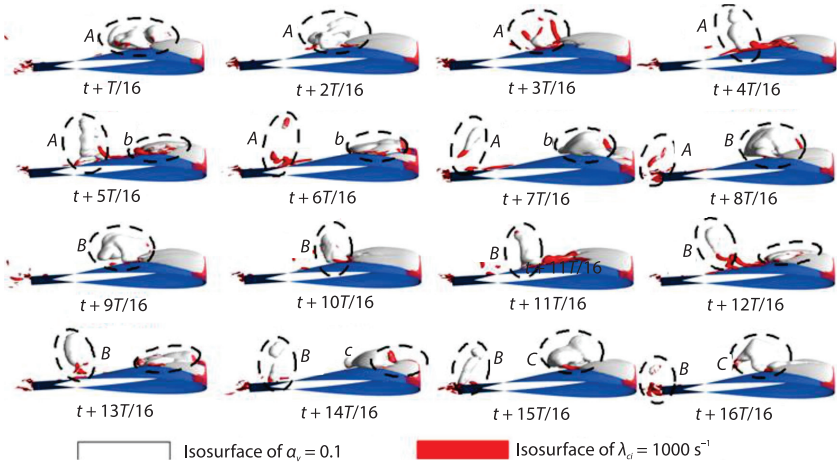

Figure 6. Simulation of cavitation evolution (front view)

The physical quantity of the cavity at each stage

According to the evolution of the Cavity A and B as show in figs. 5 and 6, the cycle of the cavity shedding around the twisted hydrofoil can be divided into six stages: Stage I, fig. 7: stability, Stage II, fig. 8: early split, Stage III, fig. 9: late split, Stage IV, fig. 7: shed, Stage V, fig. 8: *U*-shaped structure, and Stage VI, fig. 9: dissipation. The situation of the cavity at each stage is shown.

For Cavity b, it is in Stage I: stability, the Cavity A just left the main cavity which acts as a low pressure barrier to block the high pressure area at the rear of the main cavity. Due to the lack of differential pressure providing kinetic energy, there is no re-entrant jet around the main cavity cutting the main cavity. Consequently, when the previous cavity has shed, the main cavity is relatively stable, the shedding process is paused at this time, and the cavity b has not been formed.

For Cavity A, it is in Stage IV: shed. At this moment, the Cavity A is completely separated from the main cavity. The pressure on both sides of the Cavity A is relatively high, while the pressure in the center is low due to the accumulation of the cavity. Under the action of pressure gradient, the side-entrant jet flow is formed. Therefore, under the influence of the side-entrant jet, the Cavity A on either side converges towards the center. Simultaneously, the Cavity A gradually changes from the unfolding-flat shape in Stage III into the folded-wad shape in Stage IV.

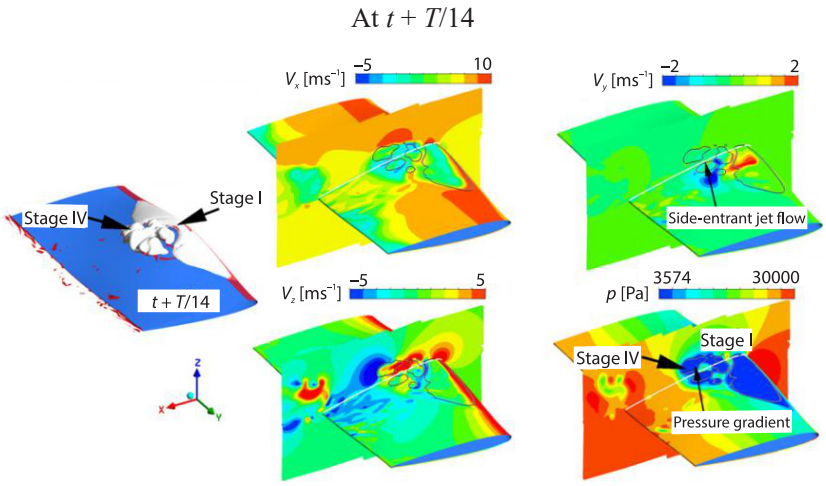

Figure 7. Cavity shedding in Stages I and IV

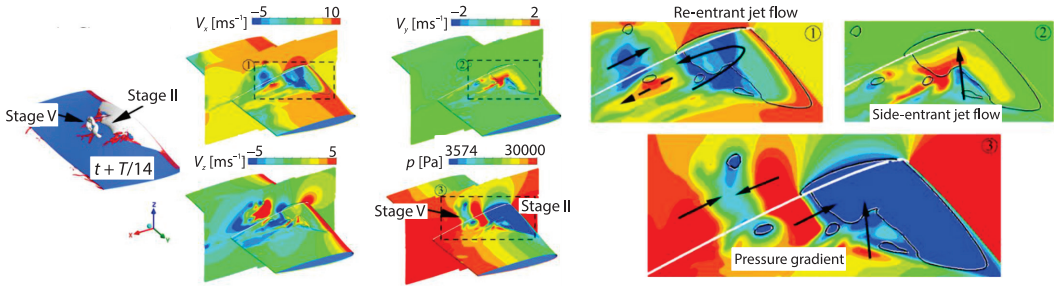

Figure. 8 Cavity shedding in Stages II an V

At $t + 4T/14$

For Cavity b, it is in Stage II: early split. At this moment, the Cavity A has left the main cavity for a certain distance. As a result, there's a high pressure zone between them, under the action of pressure gradient, the re-entrant jet flow is formed behind the main cavity. The trailing part of the Cavity B is tilted up a little bit. At the same time, the pressure gradient leads to the side-entrant jet flow cutting the main cavity. Both jets are key factors of the cavity shedding in twisted hydrofoil, and lay a foundation for the Cavity B shedding.

For Cavity A, it is in stage V: *U*-shaped structure, which is characterized by the decrease of cavity volume and the appearance of a long strip shape accompanied by stable spin, forming a stable *U*-shaped structure. The formation and effects of this structure will be mainly explained below. In Stage IV, the Cavity A was squeezed by the side-entrant jet flow on both sides, and high pressure areas appear in front and rear of the Cavity A, forming pressure difference with its own low pressure, leading to the front and rear of the Cavity A being squeezed. Therefore, the Cavity A is further squeezed from the folded round shape in Stage IV into a long strip shape in Stage V. In *X*-direction velocity cloud, itcan be seen the velocity at the top of the Cavity A is negative and at the bottom of it is positive. This is why the orientation of the Cavity A changes from the top being backward and the bottom being forward in Stage V to the top being forward and the bottom is backward in Stage VI.

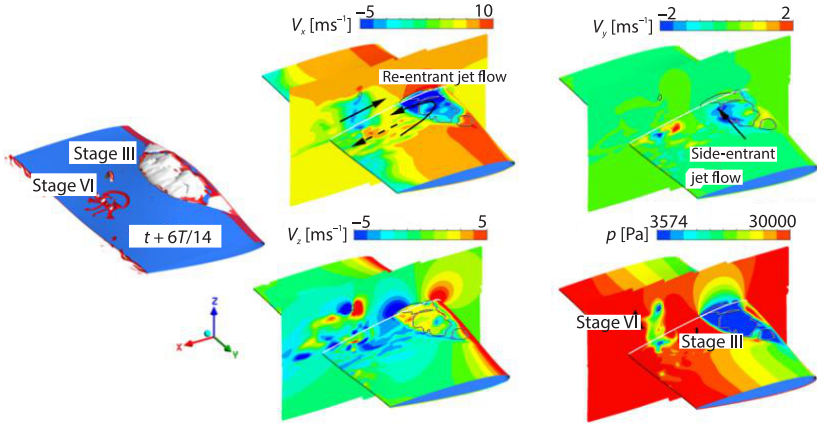

Figure 9. Cavity shedding in Stages III and VI

At $t + 6T/14$

For Cavity b, it is in Stage III: late split, with the Cavity A moving downstream, the high pressure area at the rear of the Cavity b further strengthens, so both the re-entrant and side-entrant jet flow are enhanced accordingly, and the connection between the Cavity B and the main cavity is cut off by the stronger side-entrant jet flow. Simultaneously, the Cavity B begins to be converged by the action of side-entrant jet flow, and gradually moves closer to the center. Meanwhile, the enhanced re-entrant jet makes the rear of the Cavity B lift higher, as can be seen at the corresponding time in fig. 6 that its tail has been significantly uplifted.

For Cavity A, it is in Stage VI: dissipation stage. Because the velocity on the top is lower than that on the bottom of the Cavity A, the Cavity A presents the top being forward and the bottom being backward at this moment. At the same time, under the influence of the surrounding high pressure, although the Cavity A is still protected by a certain amount of vortex at this time, the cavity has started to dissipate and is near the end of the cycle.

Re-entrant jet flow erosion

The evolution of re-entrant jet flow in the middle of the hydrofoil is shown in fig. 10. At $t + T/16 \sim t + 2T/16$, there is no strong re-entrant jet flow on the bottom of Cavity B. According to the previous study, this is because the Cavity A blocks the high pressure at the rear of hydrofoil, and the re-entrant jet flow is still concentrated on the bottom of the Cavity A. From $t + 3T/16$, the re-entrant jet flow begins to appear, and the re-entrant jet flow gradually erodes into the bottom of the Cavity B, then penetrates through the Cavity B at $t + 6T/16$. At $t + 7T/16$, the Cavity B has completely shed, and the re-entrant jet flow intensity begins to weaken. Then, the re-entrant jet flow intensity further weakened at $t + 8T/16$, and the Cavity B separates from the hydrofoil under the action of the re-entrant jet flow.

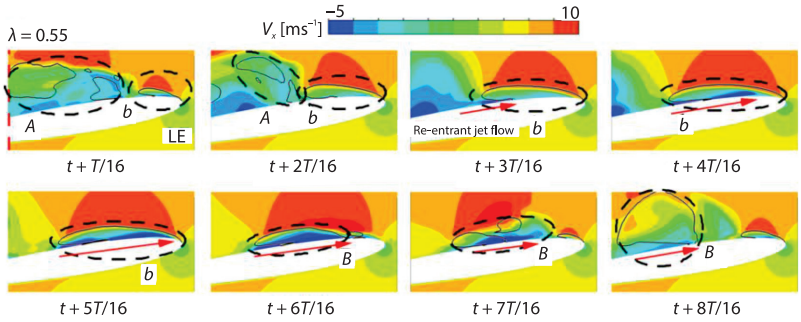

Figure 10. Flow velocity at the mid-plane

Side-entrant jet flow erosion

According to the fig. 11, from $t + 2T/16$, cracks begin to appear on the side of the Cavity B, and the shedding process of the Cavity B begins. It can be observed from the cracks of the Cavity B that there is negative velocity in Y-direction, and the side-entrant jet flow gradually goes into the interior of the Cavity B over time, and cuts off the front area of the Cavity B at $t + 6T/16$.

As the side-entrant jet flow opened cracks in the Cavity b, the re-entrant jet flow can invade the cavity from the cracks, further strengthens the erosion of the cavity, and finally makes the Cavity B shed. It can be seen that there is strong re-entrant jet flow at the cracks of the Cavity B from $t + 4T/16$ to $t + 5T/16$ in fig. 11(b).

Therefore, the main reasons for the cavity shedding around the twisted hydrofoil is caused by the combined action of the side-entrant jet flow and re-entrant jet flow, where the side-entrant jet flow affects the cutting direction, and the re-entrant jet flow is the main power source, respectively.

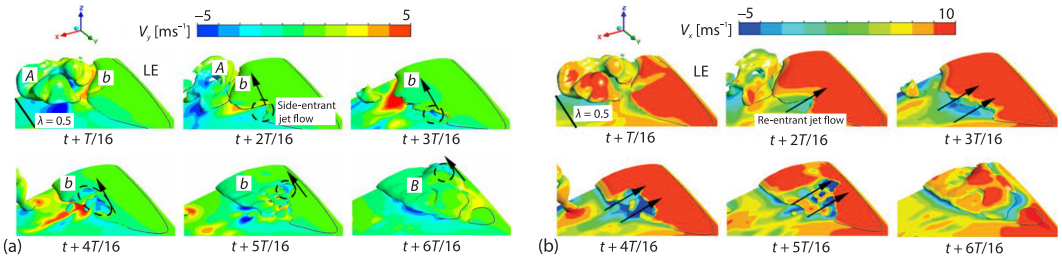

Figure 11. Velocity contour

The mechanisms of the U-shaped cavity generation

During the separation process of the Cavity b from the hydrofoil, the bottom of the Cavity b is affected by the re-entrant jet flow, which promotes the detachment of the Cavity b, and the pressure gradient exists for a long time after the cavity detachment. Since $t + 8T/16$, the rear area of the Cavity B begins to lift under the action of the re-entrant jet. As shown in fig.12(a) at $t + 9T/16$, under the combined action of the re-entrant jet flow and the mainstream on the top, the Cavity B starts to spin. In the subsequent process, the spin gradually increases, the gap in the middle region of the Cavity B increases, and the cavity gradually develops into *U*-shape structure.

As shown in fig. 12(b), at $t + 9T/16$, the Cavity B has just shed, and the strong vortex is only formed on the bottom of it. There is no strong enough vortex inside to stabilize the structure of Cavity B, and the overall structure is relatively loose. From $t + 10T/16$ to $t + 11T/16$, the Cavity B spins stronger, and the vortex inside the Cavity B also begins to increase. At $t + 37T/64$, the top of the Cavity B also appears vortex, the *U*-shaped structure gradually emerges, and the Cavity B is gradually stable. At $t + 11T/16$, the Cavity B develops into a whole *U*-shaped structure, and the vortex gets full of the Cavity B. Under the action of the *U*-shaped structure, the Cavity B is very stable, which can remain for a long time with little dissipation. Therefore, the experiment and simulation can capture the clear evolution process of the cavity structure after the Cavity B shed.

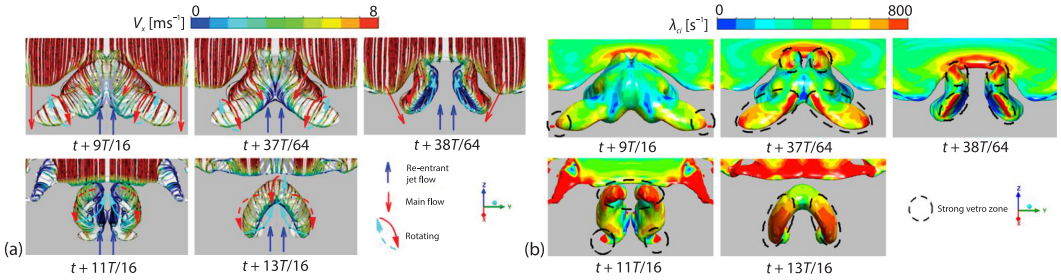

Figure 12. Mechanisms of *U*-shaped cavity formation; (a) flow velocity streamlines on *U*-shaped cavity surface and (b) vortex intensity distribution on *U*-shaped cavity surface

The change of the U-shaped cavity orientation

At $t + 11T/16$, as shown in fig. 13(a), the Cavity B is evolving towards *U*-shaped structure, and most of vapour bubbles are close to the hydrofoil surface, only the part near the center of the Cavity B is lifted up under the action of the re-entrant jet flow, as depicted in the corresponding fig. 13(b). The pressure gradient of the bottom area of the cavity is greater, so that the fluid around the bottom of Cavity B is subjected to greater resistance in the *X*-direction. Subsequently, in fig. 13(a), the flow velocity at the top of the Cavity B is greater than that on the bottom, and the orientation of the Cavity B is presented downstream.

From $t + 12T/16$ to $t + 14T/16$, due to the low density of vapour bubbles, the vapour bubbles on the bottom rise to the top region of the Cavity B, which makes the vapour bubbles in the top region more than that on the bottom. Consequently, the pressure gradient on the top is larger than that on the bottom, and the resistance is larger than that on the bottom, as shown in fig. 13(b). The flow velocity at the bottom region is large and at the top becomes lower. The top region gradually falls behind the bottom, and the orientation of the Cavity B gradually changes upstream.

At $t + 15T/16$, the Cavity B has developed to a relatively complete *U*-shaped structure and the distribution of vapour bubbles is relatively uniform, Therefore, the resistance on the top and bottom of the cavity is similar, and the surrounding flow velocity is also relatively consistent. The orientation of the Cavity B remains upstream.

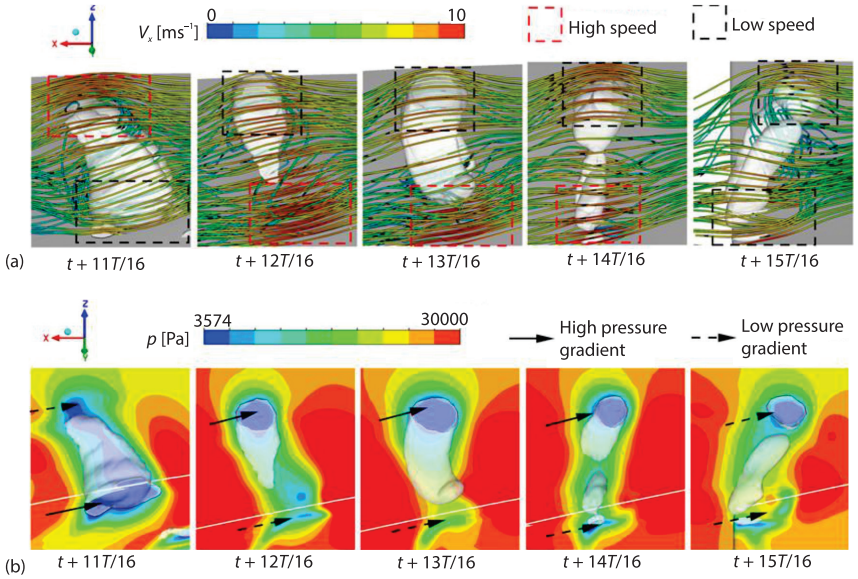

Figure 13. The phenomenon and mechanisms of orientation change of the Cavity B; (a) streamline distributionnear the shed Cavity B and (b) pressure around the shed Cavity B

Conclusion

- The shedding of cavity is periodic. When the previous cavity has just shed, the shed cavity works as a low pressure area to block the high pressure area in the rear of the main cavity, which protects the main cavity, indicating the beginning of the new cavity shedding. Simultaneously, the shedding process can be divided into six stages. stability, early split, late split, shed, *U*-shaped structure, dissipation.
- The separations of the cavity are mainly caused by the cutting of the side-entrant jet and the erosion of the re-entrant jet, in which the former provides the kinetic energy and the latter plays the role of guiding the direction. The power of the two jets are derived from the inverse pressure gradient.
- The *U*-shape structure appear after the cavity shed for a long time. Under the convective shearing action of the re-entrant jet and the main flow, the vortex is generated inside the shed cavity. Subsequently, *U*-shape structure is formed under the control of vortex.
- Most of the vapour bubbles on the bottom move to the top of the *U*-shaped cavity, because of the low density of them, which causes the magnitude of the flow velocity on the top of the *U*-shaped cavity lower than that on the bottom. Therefore, the orientation of the *U*-shaped cavity changes.

Nomenclature

C_ℓ – average lift coefficient, [–]
C_d – average drag coefficient, [–]
c – chord length, [m]
F_{vap} – evapouration coefficient, [–]
F_{cond} – condensation coefficient, [–]
k – turbulence kinetic energy, [m^2s^{-2}]
$\dot{m}^+$ – evaporation rate, [%]
$\dot{m}^-$ – condensation rate, [%]
P_k – turbulence generation term caused by viscous force, [$kgm^{-1}s^{-3}$]
P_{kb} – influence of buoyancy in k equations, [$kgm^{-1}s^{-3}$]
$P_{\varepsilon b}$ – influence of buoyancy in ε equations, [$kgm^{-1}s^{-3}$]
p – pressure, [Pa]
p_v – saturated vapour pressure, [Pa]
R_b – radius of a single bubble, [m]
T – cycle time, [s]
t – time, [s]
u – velocity, [ms^{-1}]
V – water velocity, [ms^{-1}]
V_0 – inlet velocity, [ms^{-1}]
y – wingspan, [m]

Greek symbols

α – angle of attack, [°]
α_{nuc} – nucleation site volume fraction, [–]
α_v – vapour volume fraction, [–]
ε – turbulence dissipation rate, [%]
λ_{ci} – swirling strength, [s^{-1}]
μ – dynamic viscosity, [Pa·s]
μ_t – turbulent viscosity, [Pa·s]
ρ – density, [kgm^{-3}]
σ – cavitation number, [–]

Subscripts

ℓ – liquid
v – vapour

Project funding information

This research was funded by the Qing Lan Project of Jiangsu Province, the Natural Science Foundation of the Jiangsu Higher Education Institutions of China (21KJB460026) and the industry-university-research Cooperation Project of Jiangsu Province (BY2021245).

References

[1] Foeth, E. J., *et al*., On the Collapse Structure of an Attached Cavity on a 3-D Hydrofoil, *Journal Fluids Eng*., *130* (2008), 7, 071303
[2] Foeth, E. J., The Structure of 3-D Sheet Cavitation, Ph. D. thesis, Delft University of Technology, Wageningen, The Netherlands, 2008
[3] Li, D. Q., *et al*., Towards Numerical Prediction of Unsteady Sheet Cavitation on Hydrofoils, *Journal of Hydrodynamics, Ser. B*, *22* (2010), 5, pp. 741-746
[4] Maquil, T., *et al*., The RANS Simulation of the Delft Twist 11 Foil, *Proceedings*, 2nd International Symposium on Marine Propulsors, Hamburg, Germany, 2011
[5] Bensow, R. E., Simulation of the Unsteady Cavitation on the the Delft Twist11 Foil using RANS, DES and LES, *Proceedings*, International Symposium on Marine Propulsors, Hamburg, Germany, 2011
[6] Luo, X., *et al*., Numerical Simulation of Cavity Shedding from a 3-D Twisted Hydrofoil and Induced Pressure Fluctuation by LES, *Journal Fluids Eng*., *134* (2012), 4, 04120289
[7] Ji, B., *et al*., Numerical Simulation of 3-D Cavitation Shedding Dynamics with Special Emphasis on Cavitation-Vortex Interaction, *Ocean Engineering*, *87* (2014), Sept., pp. 64-77
[8] Ji, B., *et al*., Numerical Analysis of Unsteady Cavitating Turbulent Flow and Shedding Horse-Shoe Vortex Structure Around a Twisted Hydrofoil, *Int. Journal of Multi-phase Flow*, *51* (2013), May, pp. 33-43
[9] Ji, B., *et al*., Numerical investigation of 3-D cavitation Evolution and Ex-Cited Pressure Fluctuations around a Twisted Hydrofoil, *Journal of Mechanical Science and Technology*, *28* (2014), 7, pp. 2659-2668
[10] Pan, D., Research of the Unsteady Cavitation Characteristics in Hydrofoil and Axial Flow Pump, M. Sc. thesis, Jiangsu University, Zhenjiang, China, 2015
[11] Zhang, D., *et al.*, Numerical Analysis of the Unsteady Cavitation Shedding Flow around Twisted Hydrofoil based on Hybrid Filter Model, *Thermal Science*, *22* (2018), 4, pp. 1629-1636
[12] Liu, Z., Wang, B., Numerical Simulation of the 3-D Unsteady Cavitating Flow around a Twisted Hydrofoil, *Ocean Engineering*, *188* (2019), 106313
[13] Wang, C., *et al*., Unsteady Pressure Fluctuation Characteristics in the Process of Breakup and Shedding of Sheet/Cloud Cavitation, *International Journal of Heat and Mass Transfer*, *114* (2017), Nov., pp. 769-785
[14] Cao, Y., *et al*., Numerical Study of Unsteady Cavitating Shedding Structure around a 3-D Twisted Hydrofoil, *Science Technology and Engineering*, *17* (2017), 30, pp. 1671-1815

[15] Long, X., *et al*., Large Eddy Simulation and Euler-Lagrangian Coupling Investigation of the Transient Cavitating Turbulent Flow around a Twisted Hydrofoil, *International Journal of Multi-Phase Flow*, *100* (2017), Mar., pp. 41-56
[16] Peng, X. X., *et a*l., Combined Experimental Observation and Numerical Simulation of the Cloud Cavitation with U-type Flow Structures on Hydrofoils, *International Journal of Multi-phase Flow*, *79* (2016), Mar., pp. 10-22
[17] Asnaghi, A., Bensow, R. E., Impact of Leading Edge Roughness in Cavitation Simulations around a Twisted Foil, *Fluids*, *5* (2020), 4, 243
[18] Hu, C., *et al*., Large Eddy Simulation of Turbulent Attached Cavitating Flows around Different Twisted Hydrofoils, *Energies*, *11* (2018), 10, 2768
[19] Yin, T., *et al*., Numerical Investigation of Unsteady Cavitation around a Twisted Hydrofoil, *International Journal of Multi-Phase Flow*, *135* (2021), 103506
[20] Yu, A., *et al*., Large Eddy Simulation of the Periodic Cavity Evolution and the Turbulence Characteristics around a Delft Twist-11 Hydrofoil, *Journal of Turbulence*, *21* (2020), 7, pp. 386-405
[21] Zwart, P., *et al.*, A Two-Phase Model for Predicting Cavitation Dynamics, *Proceedings*, ICMF 2014 International Conference on Multi-phase Flow, Yokohama, Japan, 2004, p. 152
[22] ***, ANSYS Inc., ANSYS CFX-Solver Theory Guide, Release 17.1, SAS IP Inc., Canonsburg, PA, USA, 2016

Paper submitted: June 6, 2022
Paper revised: September 24, 2022
Paper accepted: October 1, 2022